Scientific Research Publishing

Journal of Power and Energy Engineering, 2025, 13(8), 222-252
https://www.scirp.org/journal/jpee
ISSN Online: 2327-5901
ISSN Print: 2327-588X

# Standard Extended State Observer (SESO) and Sliding Mode Control (SMC) Combined Methods for Estimating States of the Photovoltaic (PV)/Boost Converter/DC Load System Subject to Mismatched Disturbances

**Albert Ayang[1*], Houdji Etienne Tchoffo[1,2], Jean Benjamin Bidias[1], Yaouba[1,3], Fabrice Kwefeu Mbakop[1], Guy Bertrand Tchaya[1,4]**

[1]Department of Renewable Energy, National Advance School of Engineering of Maroua, University of Maroua, Maroua, Cameroon
[2]Department of Renewable Energy, Advanced School of Mines Processing and Energy Resources, University of Bertoua, Bertoua, Cameroon
[3]Research Centre for Renewable Energy, Institute of Geological and Mining Research, Yaoundé, Cameroon
[4]Department of Renewable Energy, Faculty of Sciences, University of Dschang, Dschang, Cameroon
Email: *albertayang5@gmail.com

**How to cite this paper:** Ayang, A., Tchoffo, H.E., Bidias, J.B., Yaouba, Mbakop, F.K. and Tchaya, G.B. (2025) Standard Extended State Observer (SESO) and Sliding Mode Control (SMC) Combined Methods for Estimating States of the Photovoltaic (PV)/Boost Converter/DC Load System Subject to Mismatched Disturbances. *Journal of Power and Energy Engineering*, **13**, 222-252.
https://doi.org/10.4236/jpee.2025.138013

**Received:** June 20, 2025
**Accepted:** August 23, 2025
**Published:** August 26, 2025



## Abstract

This paper investigates the combination of the sliding mode control (SMC) and standard extended state observer (SESO) methods for estimating the states of a Photovoltaic system associated with a boost converter and DC load subject to mismatched disturbances. To assess the unknown state and the internal disturbance, including the external disturbance of the PV/Boost converter/DC Load system, the SESO based on Multiple Input Multiple Output (MIMO) systems is constructed around the nominal dynamic model for this purpose. Then, the sliding mode control is proposed to track the set references during disturbed periods. To ensure system convergence, the stability analysis of the system in the permanent regime, the extended state system, and the sliding mode control are studied. The robustness of the mixed proposed method has been tested against perturbations from the PV voltage and DC load current. It shows that the variation of the PV voltage and DC load current slightly influences the boost converter current and the DC bus voltage. On the other hand, there are gaps between the estimated and real disturbance parts (d1 and d2). However, even though the mixed methods do not accurately estimate the disturbance parts during the perturbed periods, they are robust to the studied system's principal states (inductance current IL and bus DC voltage). Further-

more, the design and dimensioning of the gains used for good state stability are more structured. The simulation results, the performance indicators and the stability analysis of the mixed methods (SESO and SMC) demonstrate the effectiveness and robustness of the principal states of the PV/Boost converter/DC Load system.

## Keywords

Standard Extended State Observer, Sliding Mode Control, Feedback Control, PV/Boost Converter/Load System, Disturbances, Perturbations

## 1. Introduction

Due to the escalating energy crisis, solar energy has emerged as the most promising renewable energy source, with photovoltaic electricity generation becoming one of the most widely utilized methods of producing renewable electricity [1]. PV systems are essential to the energy transition, providing a clean and abundant energy source [2]. PV systems are increasingly favoured for their low greenhouse gas emissions and necessitate continuous maximum power point tracking (MPPT) to maximize energy production. To track them, it must design the MPPT techniques. Several techniques and algorithms have been realized and proposed in the literature. The Perturb and Observe (P & O) [3] and Incremental conductance (IC) [4] are the most used because they are easy to implement and don't require high memory space. However, their major drawback is the speed-accuracy dilemma [5] [6]. Solar PV power generation systems are a new type of solar electrical energy generating system. They are vulnerable to the impact of solar radiation, external temperature, and seasonal changes, and many uncertainties exist [7]. Power converters have been widely used to deploy photovoltaic energy systems. They are known as systems with strong nonlinearity, uncertain parameters and disturbances [8]. PV arrays should be installed in locations that receive ample daily solar radiation. However, these optimal locations are often remote from the converter, which creates challenges for measuring PV voltage and current. Additionally, using a long cable to connect the PV arrays to the converter and DC load can lead to DC bus voltage control inaccuracies due to potential voltage drops along the cable; a boost converter (BC) connects the PV modules and the DC load. The interactions between the maximum power point tracking, boost converter, and DC load influence the system's performance [9]. Therefore, stabilising the systems' states is still challenging due to their nonlinearity, uncertain parameters, disturbances, environmental influences, and voltage drops.

In most practical projects, the classic proportional-integral (PI) controller is still used with its simple structure and easy implementation. The PI controller quickly and effectively rejects uncertain and time-varying disturbances, which degrade control performance. To overcome the external perturbations, parameter variations and measurement errors of sensors, robust controllers like the back-

stepping and sliding mode controllers (SMC) are often designed [10] [11]; They are judged to be accurate and rapid. Therefore, these controllers can efficiently improve the PV modules and obtain a PV system with good tracking performance criteria. The SMC stand out as one of the most advanced control techniques, ensuring the fulfilment of control objectives even in the presence of nonlinearities, variations in model parameters, and external disturbances. Within the realm of grid-connected converters, SMC has garnered substantial attention due to its notable attributes, including rapid dynamic response, robustness, and excellent regulation qualities [12]-[14]. This method finds significant applications in controlling grid-connected photovoltaic (PV) systems, as exemplified in [15] [16].

In recent years, active disturbance rejection control [17] (ADRC) has developed rapidly due to its strong immunity to disturbance and its independence from mathematical models of controlled objects. Its core idea is mainly through expanded state observation. The device estimates and compensates the system model and external disturbances in real time, ensuring that the system has strong anti-disturbance capabilities [18]. However, although ADRC can show good control performance in many fields, its parameter-tuning process is cumbersome, and its structure is complex. An ADRC provides robustness against uncertainties and quick disturbance response [19] [20]. The idea of ADRC is to treat all uncertainties and disturbances as a generalized disturbance and to estimate them by Extended State Observer (ESO) [21]. Then, the control scheme utilizes the uncertainties and disturbances as feedback to reduce undesired signals. Although the ADRC algorithm is easy to implement with modern digital computers, the designer is expected to deal with a set of parameters. To overcome this issue, a new approach is proposed, namely Linear Active Disturbance Rejection Control (LADRC) [22] [23], wherein a linear ESO and state feedback are used. In addition to being beneficial to its parameter adjustment, the proposal of LADRC also greatly promotes the application of active disturbance rejection control theory in engineering practice. The ADRC is also proposed and applied to the hybrid renewable energy system (HRES), and it is based on the ESO, which allows us to estimate the internal and external disturbances such as modelling errors and parameter variations [19]. Observers are designed to estimate the state or disturbance part of a system. They are designed to replace sensors in dynamics systems. There are several types of observers described in the literature, such as adaptive observers, extended state observers, sliding mode observers (SMO), unknown input observers (UIO), learning observers (LO), disturbance observers, perturbation observers, equivalent input disturbance (EID) based estimation, ESO, adaptive observer and high gain observers [24]-[33]. While some papers compare different methods, combining them in converters yields better performance than individually designed controllers [34] [35].

Standard Active Disturbance Rejection Control (SADRC) applied to the boost converter was tested by the reference [36]. The results of this work show that the standard extended state observer is robust to perturbations, but the feedback control that is used does not track the set references during the perturbed periods.

Therefore, individually, the classical method SADRC faces difficulties in maintaining the states on set references on perturbed periods. To overcome these challenges, this paper explores a combination of the SADRC and the SMC methods to estimate all system states and track the set references by rejecting perturbations. The standard extended state observer (SESO), the core of the SADRC, is formulated around the PV/Boost converter/DC Load system dynamics. The robust SMC control replaces the state feedback control law of the classic SADRC. To ensure the system's convergence, the stability analyses of the system in the permanent regime, the extended state system, and the sliding mode control are studied. The goal is to accurately estimate the system's states and return them to the references in case of external disturbances. Therefore, perturbations and uncertainties must be perfectly rejected.

This research provides several essential contributions to improving the performance of Standard Active Disturbance Rejection Control (SADRC) applied to photovoltaic systems associated with a Boost converter. The first aim is to analyze in depth the stability of the system and the impact of external perturbations on the performance of the combined SESO and SMC methods, highlighting the challenges posed by these disturbances on the stability and efficiency of the system.

The remainder of this paper is organized as follows: In Section 2, the problem is formulated by modelling both the dynamic nominal state model in the energy accumulation and transfer phases. Section 3 describes the mathematical background of the MIMO (multiple input, multiple output), SESO, and theorems that ensure their stability. Section 4 describes the construction of the SESO adapted to the PV/Boost converter/DC Load system dynamics. Section 5 outlines the stability of the studied system in the permanent regime and the stability of the SESO. The SMC law is constructed, and Lyapunov's stability analysis is studied in Section 6. Section 7 displays the simulation results of the combination methods SESO and SMC, highlighting the effectiveness and robustness of the proposed method in perturbed periods. Finally, we conclude the work in Section 8.

## 2. Problem Formulation and Model Dynamics

### 2.1. Dynamic Nominal State Model

In this work, a boost controller is used as the converter; its structure is illustrated in Figure 1. Power converters' dynamic models are most often nonlinear.

With such a converter, the goal is to establish an average voltage, $V_{bus\_DC\_ref}$, at the converter output that meets the following criteria: $V_{bus\_DC\_ref} \succ V_{PV}$ and $V_{bus\_DC\_ref}$ is adjustable.

It is assumed that the voltage from the PV is the voltage $V_{mp}$ at the maximum power point, obtained by the "perturb and observe" control [37].

#### 2.1.1. Energy Accumulation Phase in the Smoothing Inductor $L_{PV}$

For the duty cycle $\mu = 1$ switch $ST$ is closed and the diode $D$ is open. During this phase, the inductor $L_{PV}$ starts to accumulate energy. Indeed, the induc-

tor is subjected to a constant voltage source $V_{PV}$. The transfer diode $D$ is blocked and the capacitor $C_{dc}$, initially charged, slowly discharges into the load $I_{load}$; the equivalent circuit is illustrated in Figure 2.

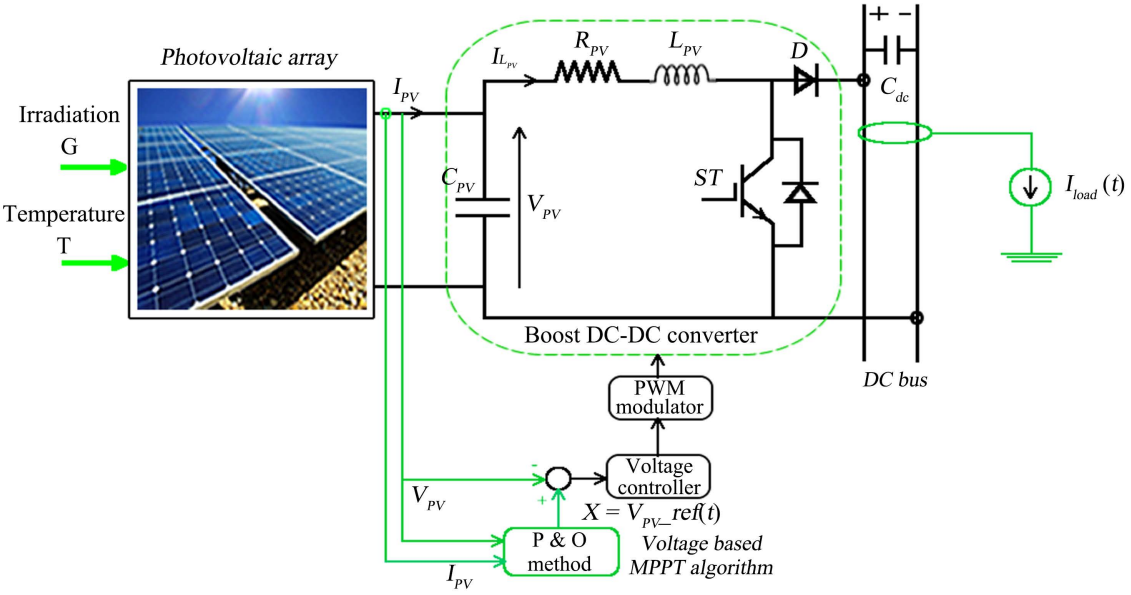


Figure 1. DC-DC converter and load integrated into the photovoltaic system.

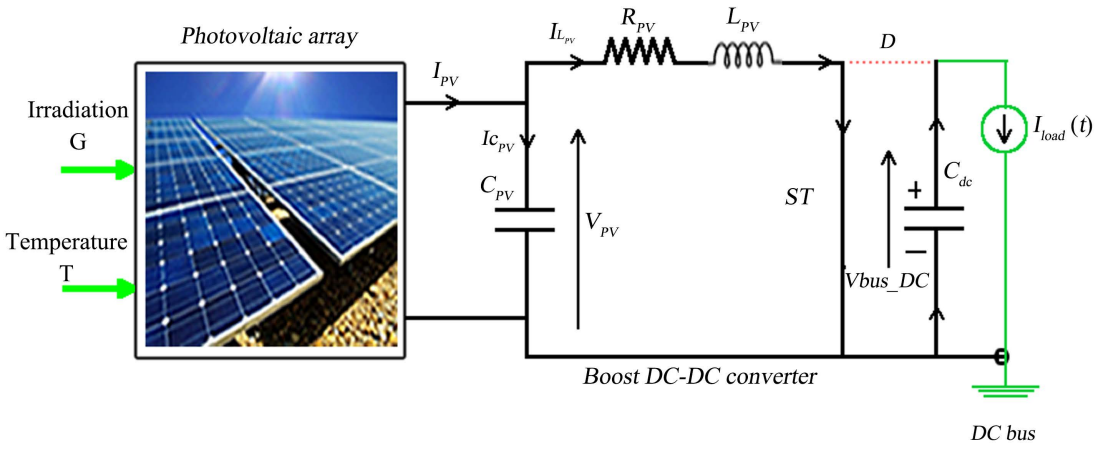


Figure 2. Energy accumulation phase.

The dynamic model for this phase is written as follows:

$$\begin{cases} \dfrac{\mathrm{d}I_{L_{pv}}}{\mathrm{d}t} = \dfrac{-R_{pv}}{L_{pv}} I_{L_{pv}} + \dfrac{V_{pv}}{L_{pv}} \\ \dfrac{\mathrm{d}V_{bus\_dc}}{\mathrm{d}t} = -\dfrac{1}{C_{dc}} I_{load} \end{cases} \tag{1}$$

### 2.1.2. Energy Transfer Phase

For the duty cycle $\mu = 0$ the switch $ST$ is open and the diode $D$ is closed. Diode D starts to conduct to ensure the continuity of the current in the inductor

$L_{PV}$ . The energy accumulated by the inductor is then transferred to the load and to the capacitor which renews its voltage. The equivalent circuit is shown in Figure 3.

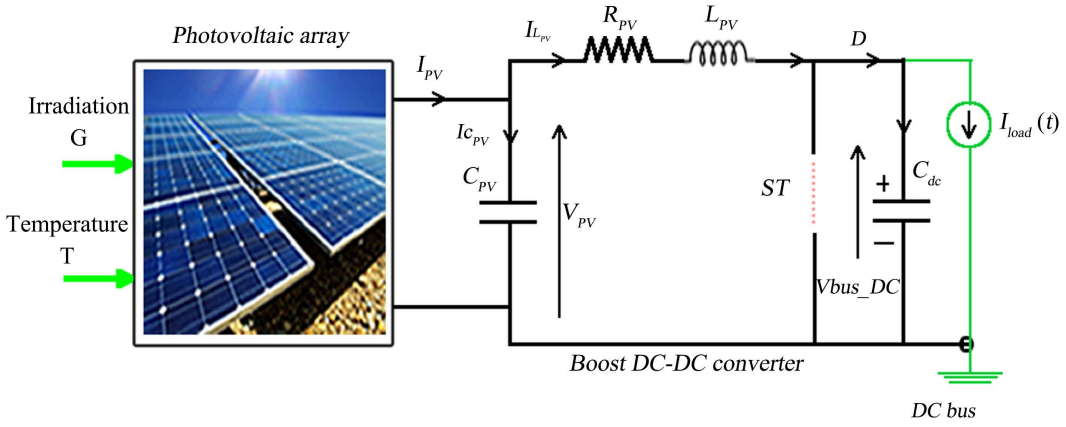


**Figure 3.** Energy transfer phase.

The dynamic model for this phase is written as follows:

$$\begin{cases} \dfrac{\mathrm{d}I_{L_{pv}}}{\mathrm{d}t} = \dfrac{-R_{pv}}{L_{pv}} I_{L_{pv}} + \dfrac{V_{pv}}{L_{pv}} - \dfrac{V_{bus\_DC}}{L_{pv}} \\ \dfrac{\mathrm{d}V_{bus\_DC}}{\mathrm{d}t} = -\dfrac{1}{C_{dc}} I_{load} + \dfrac{I_{L_{pv}}}{C_{dc}} \end{cases} \tag{2}$$

When the switching frequency is high, it is possible to model the average dynamic behavior of these converters [38] [39]. Combining the subsystems of Equations (1) and (2), we obtain the average dynamic model of the system:

$$\begin{cases} \dfrac{\mathrm{d}I_{L_{pv}}}{\mathrm{d}t} = \dfrac{-R_{pv}}{L_{pv}} I_{L_{pv}} + \dfrac{V_{pv}}{L_{pv}} - \dfrac{(1-\mu)}{L_{pv}} V_{bus\_DC} \\ \dfrac{\mathrm{d}V_{bus\_DC}}{\mathrm{d}t} = \dfrac{(1-\mu)}{C_{dc}} I_{L_{pv}} - \dfrac{1}{C_{dc}} I_{load} \end{cases} \tag{3}$$

With $\mu \in [0,1]$.

By putting $x_1 = I_{L_{pv}}$ et $x_2 = V_{bus\_DC}$, Equation (3) takes the following form:

$$\dot{x}(t) = Ax(t) + g(x) \cdot \mu + E_d \cdot d \tag{4}$$

With $A = \begin{pmatrix} -R_{pv}/L_{pv} & -1/L_{pv} \\ 1/C_{dc} & 0 \end{pmatrix}$, $g(x) = \begin{pmatrix} x_2(t)/L_{pv} \\ -x_1(t)/C_{pv} \end{pmatrix}$, $E_d = I_{2x2}$,

$d = \begin{pmatrix} V_{pv}/L_{pv} \\ -I_{load}/C_{dc} \end{pmatrix}$.

Equation (4) represents the nonlinear dynamic model of the system under investigation.

## 3. Mathematical Background

**Remark 1**: A matrix A is Hurwitz if it is square, and all real parts of its eigen-

values are strictly negative. System or subsystem with A as state matrix is stable.

**Assumption 1** [40]: Consider the MIMO (multiple input multiple output) system below with considerable uncertainties and disturbances.

$$\begin{cases} x_1^{(n_1)}(t) = f_1\left(x_1(t),\cdots,x_1^{(n_1-1)}(t),\cdots,x_m^{(n_m-1)}(t),w_1(t)\right)+g_1\left(u_1(t),\cdots,u_k(t)\right), \\ x_2^{(n_2)}(t) = f_2\left(x_1(t),\cdots,x_1^{(n_1-1)}(t),\cdots,x_m^{(n_m-1)}(t),w_2(t)\right)+g_2\left(u_1(t),\cdots,u_k(t)\right), \\ \quad\vdots \\ x_m^{(n_m)}(t) = f_m\left(x_1(t),\cdots,x_1^{(n_1-1)}(t),\cdots,x_m^{(n_m-1)}(t),w_m(t)\right)+g_m\left(u_1(t),\cdots,u_k(t)\right), \\ y_i(t) = x_i(t), i=1,2,\cdots,m. \end{cases} \tag{5}$$

$f_i$ represents the non-linear function of the system, $w_i(t)$ external disturbances, $u_i(t)$ the controls, $y_i(t)$ the outputs of the system, and $g_i \in C\left(\mathbb{R}^k,\mathbb{R}\right)$.

For all $i \in \{1,2,\cdots,m\}$, all $u_i(t)$, $w_i(t)$, $\dot{w}_i(t)$, and MIMO solutions are bounded; $g_i \in C\left(\mathbb{R}^k,\mathbb{R}\right)$, $f_i \in C^1\left(\mathbb{R}^{n_1+\cdots+n_m+1},\mathbb{R}\right)$.

**Assumption 2** [40]: For all $i \in \{1,2,\cdots,m\}$, there are positive constants $\lambda_{i,j}$ $\left(j=1,2,\cdots,m\right)$, $\beta_i$, and positive functions $V_i$, $W_i$: $\mathbb{R}^{n_i+1} \to \mathbb{R}$ that satisfy the following conditions:

- $\lambda_{i,1}\|y\|^2 \le V_i(y) \le \lambda_{2,i}\|y\|^2$, $\lambda_{i,3}\|y\|^2 \le W_i(y) \le \lambda_{4,i}\|y\|^2$,
- $\sum_{l=1}^{n_i} \frac{\partial V_i(y)}{\partial y_l}\left(y_{l+1}-\varphi_{i,l}(y_1)\right) - \frac{\partial V(y)}{\partial y_{n_i+1}}\varphi_{i,n_i+1}(y_1) \le -W_i(y)$
- $\left|\frac{\partial V_i(y)}{\partial y_{n_i+1}}\right| \le \beta_i\|y\|$, $\forall\, y=\left(y_1,y_2,\cdots,y_{n+1}\right)$

**Theorem 1** [40]: Based on assumptions 1 and 2, for all given initial values of the MIMO

For any positive constant $a>0$,

$$\lim_{\tau\to 0}\left|x_{i,j}(t)-\hat{x}_{i,j}(t)\right| = 0 \quad \text{uniformly for} \quad t \in [a,\infty);$$

There is $\tau_0 > 0$ such that for each $\tau \in (0,\tau_0)$ there exists $t_\tau > 0$ as

$$\left|x_{i,j}(t)-\hat{x}_{i,j}(t)\right| \le K_{ij}\tau^{n_i+2-j}, \quad t \in (t_\tau,\infty).$$

A typical example of Standard Extended State Observer (SESO) satisfying the conditions of the theorem is a Linear Extended State Observer (LESO) of the following form:

$$\begin{cases} \dot{\hat{x}}_{i,1}(t) = \hat{x}_{i,2}(t) + \frac{1}{\tau}k_{i,1}\left(x_{i,1}(t)-\hat{x}_{i,1}(t)\right) \\ \dot{\hat{x}}_{i,2}(t) = \hat{x}_{i,3}(t) + \frac{1}{\tau^2}k_{i,2}\left(x_{i,1}(t)-\hat{x}_{i,1}(t)\right) \\ \quad\vdots \\ \dot{\hat{x}}_{i,n_i}(t) = \hat{x}_{i,n_i+1}(t) + \frac{1}{\tau^{n_i}}k_{i,n_i}\left(x_{i,1}(t)-\hat{x}_{i,1}(t)\right) + g_i\left(u_1(t),u_2(t),\cdots,u_k(t)\right) \\ \dot{\hat{x}}_{i,n_i+1}(t) = \frac{1}{\tau^{n_i+1}}k_{i,n_i+1}\left(x_{i,1}(t)-\hat{x}_{i,1}(t)\right), i=1,2,\cdots,m. \end{cases} \tag{6}$$

$$E_i = \begin{pmatrix} -k_{i,1} & 1 & 0 & \cdots & 0 \\ -k_{i,2} & 0 & 1 & \cdots & 0 \\ \vdots & \vdots & \vdots & \ddots & \vdots \\ -k_{i,n_i} & 0 & 0 & \cdots & 1 \\ -k_{i,n_i+1} & 0 & 0 & \cdots & 0 \end{pmatrix}$$

All matrices are assumed to be Hurwitz and assumptions 1 and 2 are satisfied.

## 4. Standard Extended State Observer

By setting the reference state variables $i_{L_{pv}\_ref} = x_{1\_ref}(t)$ and $V_{bus\_DC\_ref} = x_{2\_ref}(t)$, Equation (3) can be rewritten in the following form:

$$\begin{cases} \dot{x}_1(t) = \dfrac{-R_{pv}}{L_{pv}} x_1(t) - \dfrac{1}{L_{pv}} x_2(t) + \dfrac{x_{2\_ref}(t)}{L_{pv}}\mu + \left[\dfrac{V_{pv}}{L_{pv}} + \left(\dfrac{1}{L_{pv}} x_2(t) - \dfrac{x_{2\_ref}(t)}{L_{pv}}\right)\mu\right] \\ \dot{x}_2(t) = \dfrac{1}{C_{dc}} x_1(t) - \dfrac{x_{1\_ref}(t)}{C_{dc}}\mu + \left[-\dfrac{1}{C_{dc}} I_{load} + \left(-\dfrac{1}{C_{dc}} x_1(t) + \dfrac{x_{1\_ref}(t)}{C_{dc}}\right)\mu\right] \end{cases} \quad (7)$$

By putting $U = \begin{pmatrix} U_1 \\ U_2 \end{pmatrix} = \begin{pmatrix} x_{2\_ref}(t)\mu \\ x_{1\_ref}(t)\mu \end{pmatrix}$ as the control of the system, and

$$d(x,u,t) = \begin{pmatrix} d_1(x,u,t) \\ d_2(x,u,t) \end{pmatrix} = \begin{pmatrix} \dfrac{V_{pv}}{L_{pv}} + \left(\dfrac{1}{L_{pv}} x_2(t) - \dfrac{x_{2\_ref}(t)}{L_{pv}}\right)\mu \\ -\dfrac{1}{C_{dc}} I_{load} + \left(-\dfrac{1}{C_{dc}} x_1(t) + \dfrac{x_{1\_ref}(t)}{C_{dc}}\right)\mu \end{pmatrix}$$

a nonlinear function representing the nonlinearity and the parts likely to be disturbed of the subsystem, Equation (7) becomes:

$$\begin{cases} \dot{x}_1(t) = \dfrac{-R_{pv}}{L_{pv}} x_1(t) - \dfrac{1}{L_{pv}} x_2(t) + \dfrac{1}{L_{pv}} U_1(t) + d_1(x,u,t) \\ \dot{x}_2(t) = \dfrac{1}{C_{dc}} x_1(t) + \left(-\dfrac{1}{C_{dc}}\right) U_2(t) + d_2(x,u,t) \end{cases} \quad (8)$$

By putting $b_{1,0} = \dfrac{1}{L_{pv}}$ and $b_{2,0} = -\dfrac{1}{C_{dc}}$, Equation (9) becomes:

$$\begin{cases} \dot{x}_1(t) = \dfrac{-R_{pv}}{L_{pv}} x_1(t) - \dfrac{1}{L_{pv}} x_2(t) + b_{1,0} U_1(t) + d_1(x,u,t) \\ \dot{x}_2(t) = \dfrac{1}{C_{dc}} x_1(t) + b_{2,0} U_2(t) + d_2(x,u,t) \end{cases} \quad (9)$$

So, disturbances $d_1$ are affected by the parameters $V_{pv}$, $L_{pv}$, state $x_2$ and by the duty cycle $\mu$; and disturbances $d_2$ are affected by the parameters $I_{load}$, $C_{dc}$, state $x_1$ and by the duty cycle $\mu$.

The Equation (9) takes the form of a MIMO system presented in Equation (5). Thus, we have a MIMO system, and referring to Equation (6), then the standard extended state observer of the system takes the following form:

$$\begin{cases} \dot{\hat{x}}_1(t) = \hat{d}_1 + \dfrac{-R_{pv}}{L_{pv}}\hat{x}_1(t) - \dfrac{1}{L_{pv}}\hat{x}_2(t) + b_{1,0}\cdot U_1(t) + \dfrac{k_1}{\varepsilon_1^2}\left(x_1(t) - \hat{x}_1(t)\right) \\ \dot{\hat{d}}_1 = \dfrac{k_2}{\varepsilon_1^3}\left(x_1(t) - \hat{x}_1(t)\right) \\ \dot{\hat{x}}_2(t) = \hat{d}_2 + \dfrac{1}{C_{dc}}\hat{x}_1(t) + b_{2,0}\cdot U_2(t) + \dfrac{k_3}{\varepsilon_2^2}\left(x_2(t) - \hat{x}_2(t)\right) \\ \dot{\hat{d}}_2 = \dfrac{k_4}{\varepsilon_2^3}\left(x_2(t) - \hat{x}_2(t)\right) \end{cases} \tag{10}$$

$k_1$, $k_2$, $k_3$, $k_4 \in \mathbb{R}^+$; $\varepsilon \in (0, \varepsilon_0)$.

By properly choosing the coefficients $k_1$, $k_2$, $k_3$, $k_4$ of matrix $E_1 = \begin{pmatrix} -k_1 & 1 \\ -k_2 & 0 \end{pmatrix}$ and $E_2 = \begin{pmatrix} -k_3 & 1 \\ -k_4 & 0 \end{pmatrix}$, so that they are Hurwitz, Equation (10) estimates the state variables $x_1$ and $x_2$, and disturbances $d_1(x,u,t)$ and $d_2(x,u,t)$. The standard extended state observer is designed to estimate all state variables and disturbances.

**Theorem 2**: By appropriately choosing the observer's gain $E_1$ and $E_2$, the stability of Equation (10) is guaranteed under the assumption that $d_1(t)$ et $d_2(t)$ are bounded [41].

## 5. Stability Analysis

### 5.1. Stability Analysis of the Nominal System in Steady State

Let's put $\zeta(t) = \begin{pmatrix} \zeta_1(t) \\ \zeta_2(t) \end{pmatrix} = \begin{pmatrix} x_1(t) - x_{1\_ref}(t) \\ x_2(t) - x_{2\_ref}(t) \end{pmatrix}$ the error between the nominal states and the set references.

The dynamic of the error becomes:

$$\dot{\zeta}(t) = \begin{pmatrix} \dot{x}_1(t) \\ \dot{x}_2(t) \end{pmatrix} = \begin{pmatrix} \dfrac{-R_{pv}}{L_{pv}}\left(\zeta_1(t) + x_{1\_ref}(t)\right) - \dfrac{(1-\mu)}{L_{pv}}\left(\zeta_2(t) + x_{2\_ref}(t)\right) + \dfrac{V_{pv}}{L_{pv}} \\ \dfrac{(1-\mu)}{C_{dc}}\left(\zeta_1(t) + x_{1\_ref}(t)\right) - \dfrac{1}{C_{dc}}I_{load} \end{pmatrix} \tag{11}$$

In steady state $\dot{\zeta}(t) = \zeta(t) = 0_{2x1}$, thus:

$$\begin{pmatrix} \dfrac{-R_{pv}}{L_{pv}}x_{1\_ref}(t) - \dfrac{(1-\mu)}{L_{pv}}x_{2\_ref}(t) + \dfrac{V_{pv}}{L_{pv}} \\ \dfrac{(1-\mu)}{C_{dc}}x_{1\_ref}(t) - \dfrac{1}{C_{dc}}I_{load} \end{pmatrix} = \begin{pmatrix} 0 \\ 0 \end{pmatrix} \tag{12}$$

At high frequencies $\mu$ is a constant. Thus, the PV voltage and the load current are expressed as:

$$\begin{pmatrix} V_{pv} \\ I_{load} \end{pmatrix} = \begin{pmatrix} R_{pv}x_{1\_ref}(t) + (1-\mu)x_{2\_ref}(t) \\ (1-\mu)x_{1\_ref}(t) \end{pmatrix} \tag{13}$$

*The Equation (13) allows suitable choices of PV voltage and load current values*

*to be made according to the duty cycle and set references* $x_{1\_ref}(t)$, *and* $x_{2\_ref}(t)$. *This Equation* (*13*) *ensures the stability of the nominal state system.*

## 5.2. Stability Analysis of the Extended State System

Let's put the estimation error $e(t)=\begin{pmatrix} e_1(t) \\ e_2(t) \\ e_3(t) \\ e_4(t) \end{pmatrix}=\begin{pmatrix} x_1(t)-\hat{x}_1(t) \\ x_2(t)-\hat{x}_2(t) \\ d_1(t)-\hat{d}_1(t) \\ d_2(t)-\hat{d}_2(t) \end{pmatrix}$.

The dynamics of the estimation error are written as:

$$\dot{e}(t)=\begin{pmatrix} \dot{e}_1(t) \\ \dot{e}_2(t) \\ \dot{e}_3(t) \\ \dot{e}_4(t) \end{pmatrix}=\begin{pmatrix} \dot{x}_1(t)-\dot{\hat{x}}_1(t) \\ \dot{x}_2(t)-\dot{\hat{x}}_2(t) \\ \dot{d}_1(t)-\dot{\hat{d}}_1(t) \\ \dot{d}_2(t)-\dot{\hat{d}}_2(t) \end{pmatrix} \tag{14}$$

$$\dot{e}(t)=\begin{pmatrix} \dfrac{-R_{pv}}{L_{pv}}\left(x_1(t)-\hat{x}_1(t)\right)-\dfrac{1}{L_{pv}}\left(x_2(t)-\hat{x}_2(t)\right)-\dfrac{k_1}{\varepsilon_1^2}\left(x_1(t)-\hat{x}_1(t)\right)+\left(d_1-\hat{d}_1\right) \\ \dfrac{1}{C_{dc}}\left(x_1(t)-\hat{x}_1(t)\right)-\dfrac{k_3}{\varepsilon_2^2}\left(x_2(t)-\hat{x}_2(t)\right)+\left(d_2-\hat{d}_2\right) \\ \dot{d}_1-\dfrac{k_2}{\varepsilon_2^2}\left(x_1(t)-\hat{x}_1(t)\right) \\ \dot{d}_2-\dfrac{k_4}{\varepsilon_4^2}\left(x_2(t)-\hat{x}_2(t)\right) \end{pmatrix} \tag{15}$$

In state matrix form, the dynamic error is written as:

$$\dot{e}(t)=\Gamma e+Eh(t) \tag{16}$$

With

$$\Gamma=\begin{pmatrix} -\dfrac{R_{pv}}{L_{pv}}-\dfrac{k_1}{\varepsilon_1^2} & -1/L_{pv} & 1 & 0 \\ \dfrac{1}{C_{dc}} & -\dfrac{k_3}{\varepsilon_3^2} & 0 & 1 \\ -\dfrac{k_2}{\varepsilon_2^2} & 0 & 0 & 0 \\ 0 & -\dfrac{k_4}{\varepsilon_4^2} & 0 & 0 \end{pmatrix},\quad E=\begin{pmatrix} 0 & 0 \\ 0 & 0 \\ 1 & 0 \\ 0 & 1 \end{pmatrix},\quad h(t)=\begin{pmatrix} \dot{d}_1(t) \\ \dot{d}_2(t) \end{pmatrix}$$

The dynamic error solution becomes:

$$e(t)=\exp(\Gamma t)e(0)+Eh(t)\int_0^t \exp\left(\Gamma(t-\tau)\right)\mathrm{d}\tau \tag{17}$$

where $e(0)$ is the initial estimate error.

*The stability of the extended state system is based on the stability of the matrix* $\Gamma$. *Thus, the extended state system is stable if and only if* $\Gamma$ *is a Hurwitz matrix.*

## 6. Control Law by Sliding Mode Control

In this work, the sliding mode control is used to track the set references of the system. It is known as a robust control in the literature.

### 6.1. Sliding Mode Control Law

Equation (4) can be rewritten in the following form:

$$\dot{x}(t) = f(x) + g_1(x)u(t) + g_2(x)d(t) \tag{18}$$

With, $f(x) = Ax(t)$, $g_1(x) = B$, $g_2(x) = E_d$

The estimated state equation is written:

$$\dot{\hat{x}}(t) = f(\hat{x}) + g_1(\hat{x})u(t) + g_2(\hat{x})\hat{d}(t) \tag{19}$$

Either:

$$s = \hat{e} + \beta\int \hat{e}\mathrm{d}t \tag{20}$$

The sliding surface of the integral form [42], with $\hat{e} = \hat{x} - x_d$ being the error at the states, $\hat{x}$ the estimated states, and $x_d$ the states desired by the system control.

By deriving the sliding surface $\dot{s} = \dot{\hat{e}} + \beta\hat{e} = \left(\dot{\hat{x}} - \dot{x}_d\right) + \beta\left(\hat{x} - x_d\right)$ and combining it with Equation (13), we obtain:

$$\dot{s} = 0 \Rightarrow \left(\dot{\hat{x}} - \dot{x}_d\right) + \beta\left(\hat{x} - x_d\right) = 0 \Rightarrow f(\hat{x}) + g_1(\hat{x})u(t) + g_2(\hat{x})\hat{\hat{d}}(t) - \dot{x}_d + \beta\hat{e} = 0$$

So, the control becomes:

$$u^*(t) = \left(g_1(\hat{x})\right)^{-1}\left[\dot{x}_d - \beta\hat{e} - f(\hat{x}) - g_2(\hat{x})\cdot\hat{d}(t) - K\cdot sign(s) - s\frac{\left|g_2(\hat{x})\right|^2}{\eta(\hat{x})}\right] \tag{21}$$

With $\eta > 0$, $\beta > 0$, $K > D_{\sup}$, $\hat{d}(t)$ are bounded perturbations and $\left|\hat{d}(t)\right| \le D_{\sup}$, $\hat{e} = \begin{pmatrix}\hat{e}_1\\ \hat{e}_2\end{pmatrix}$.

$\hat{x}$ and $\hat{d}(t)$ are estimated by the standard extended state observer.

Figure 4 schematically shows the block diagram of the implementation of the standard extended state observer (SESO) and Sliding Mode Control (SMC) combination methods.

**Hypothesis 3:** The disturbances and their derivatives are bounded, and have constant values in steady state, so:

$$\lim_{t\to\infty}\dot{d}(t,x,u) = 0 \quad \text{and} \quad \lim_{t\to\infty} d(t,x,u) = \sup\left|d(t,x,u)\right|$$

### 6.2. Stability Analysis by Lyapunov

Consider the following Lyapunov function:

$$V = \frac{1}{2}s^2 \tag{22}$$

The derivative of the Lyapunov function gives:

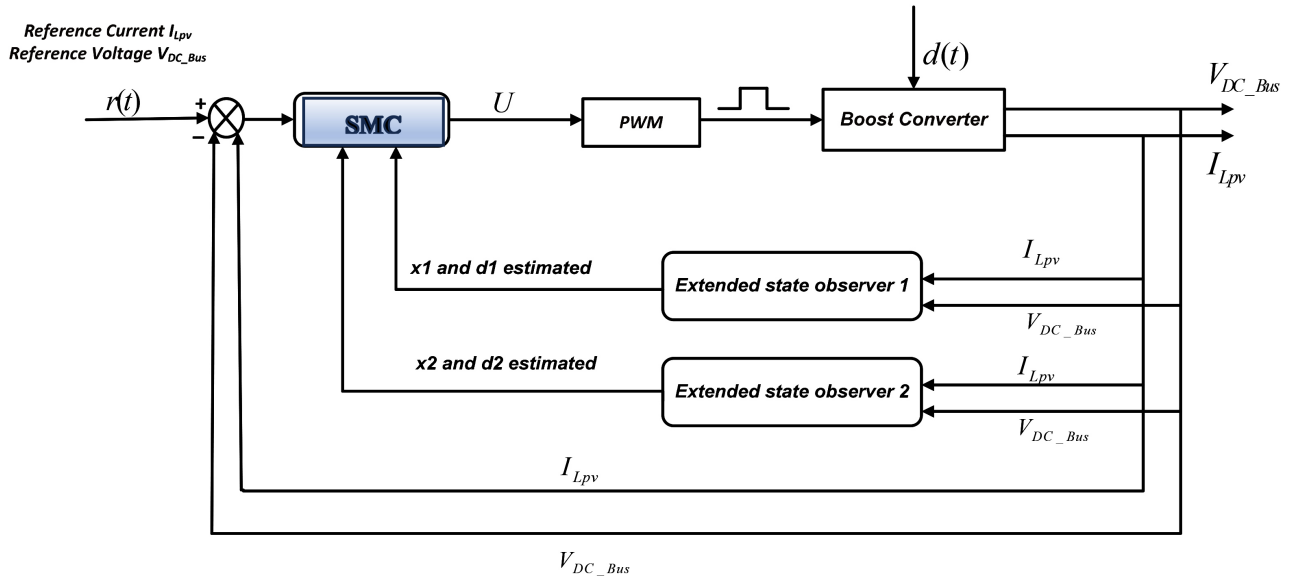


**Figure 4.** Block diagram of the SESO and SMC combination methods for estimating states and controlling the PV/Boost converter/Load system.

$$\dot{V} = \dot{s}s \tag{23}$$

Considering Equations (18) to (21):

$$\begin{aligned} \dot{V} &= s\left(\beta\hat{e} + \left(\dot{\hat{x}} - \dot{x}_d\right)\right) \\ &= s\left(\beta\hat{e} + f\left(\hat{x}\right) + g_1\left(\hat{x}\right)u\left(t\right) + g_2\left(\hat{x}\right)\hat{d}\left(t\right) - \dot{x}_d\right) \end{aligned} \tag{24}$$

Given that $g_1\left(\hat{x}\right)u\left(t\right) = \dot{x}_d - \beta\hat{e} - f\left(\hat{x}\right) - g_2\left(\hat{x}\right)\cdot\hat{d}\left(t\right) - K\cdot sign\left(s\right) - s\dfrac{\left|g_2\left(\hat{x}\right)\right|^2}{\eta\left(\hat{x}\right)}$

$$\begin{aligned} \dot{V} = s\Bigg( & \beta\hat{e} + f\left(\hat{x}\right) + \dot{x}_d - \beta\hat{e} - f\left(\hat{x}\right) - g_2\left(\hat{x}\right)\cdot\hat{d}\left(t\right) - K\cdot sign\left(s\right) \\ & - s\frac{\left|g_2\left(\hat{x}\right)\right|^2}{\eta\left(\hat{x}\right)} + g_2\left(\hat{x}\right)\hat{d}\left(t\right) - \dot{x}_d\Bigg) \\ = s\Bigg( & -K\cdot sign\left(s\right) - s\frac{\left|g_2\left(\hat{x}\right)\right|^2}{\eta\left(\hat{x}\right)}\Bigg) \end{aligned} \tag{25}$$

So,

$$\dot{V} \le -\left|s\right|k - \left|s\right|^2\frac{\left|g_2\left(\hat{x}\right)\right|^2}{\eta\left(\hat{x}\right)} \tag{26}$$

Or $K > 0$ and $\eta\left(\hat{x}\right) > 0$, so for everything $s \neq 0$:

$$\dot{V} < 0 \tag{27}$$

Which means $\lim_{t\to\infty}\left(s\right) \approx 0$.

The sliding surface is thus reached, and steady-state stability is ensured by the sliding surface (22).

## 7. Assumptions and Limitations

- The non-linear components of the dynamic model are treated as disturbances;
- The PV voltage and the load current without variations are considered as nominal without perturbations;
- The references or targets limits are defined in steady state;
- It is assumed that the chopper switch ST is ideal, does not fail and the functional temperature is constant;
- It is assumed that the system's output measurement sensors are functioning without faults.

## 8. Simulation Results

### 8.1. Studied System Parameters

The mixed of the sliding mode control (SMC) and standard extended state observer (SESO) approaches applied to the Photovoltaic system associated with a boost converter and DC load, subject to mismatched disturbances, has been implemented and validated by Matlab/Simulink software according to the parameters shown in Table 1. The Boost parameters, PV voltage, and DC bus voltage are taken from work done by Palak Jain *et al.* [43].

**Table 1.** Simulation parameters [43].

| Parameter | Value |
|---|---|
| Bus reference voltage, Vdc_bus_ref | 240 V |
| Reference inductance current, IL_ref | 12 A |
| Input voltage of the PV array system assumed to be fixed, Vpv | 120 V |
| Load current assumed fixed, Iload | 12 A |
| Chopper inductance, Lpv | 0.005 H |
| Chopper capacitance load input, Cdc | 0.00285 F |
| Chopper resistance, Rpv | 1 Ω |
| PWM parameters: Switching frequency and sampling step | f = 10,000 Hz<br>P = 0.00001 s |

By correctly choosing the parameters of the standard extended state observer of Equation (15), such as: $\varepsilon_1 = 0.0065$ $\varepsilon_2 = 0.0095$ and $E_1 = E_2 = \begin{pmatrix} -3 & 1 \\ -1 & 0 \end{pmatrix}$.

The eigenvalues of $E_1$ and $E_2$ are $\{-2,6180; -0,3820\}$. These eigenvalues are strictly negative real decimal numbers.

Thus, the solutions of the standard extended state observer (Equation (10)) are stable.

The sliding mode control parameters are as follows:

$$K = \begin{bmatrix} K_1 \\ K_2 \end{bmatrix} = \begin{bmatrix} 40000 \\ 19100 \end{bmatrix} > \begin{bmatrix} |V_{pv}/L_{pv}| \\ |-I_{load}/C_{dc}| \end{bmatrix}, \quad \beta = \begin{pmatrix} 30 \\ 30 \end{pmatrix}, \quad \eta(x) = \begin{pmatrix} \eta_1 \\ \eta_2 \end{pmatrix} = \begin{pmatrix} 2 \\ 1 \end{pmatrix},$$

$$c_{01}=5\times10^{-6},\ s_{01}=e_{01},\ c_{02}=5\times10^{-6},\ s_{02}=e_{02},\ s=\begin{pmatrix}s_1\\s_2\end{pmatrix}=\begin{pmatrix}c_{01}\cdot s_{01}+e_1\\c_{02}\cdot s_{02}+e_2\end{pmatrix}$$

## 8.2. States Estimation Results without External Perturbations

Figure 5 illustrates the actual inductance current alongside its estimated value generated by the combination of SMC and SESO. The estimated error ranges from 0.0 A to 0.5 A, resulting in a relative error of 4%. This indicates that the estimated values are close to the actual values. The results demonstrate that the estimator accurately predicts the current, allowing effective tracking of the set reference, even when the current peaks around 190 A at the beginning of the simulation.

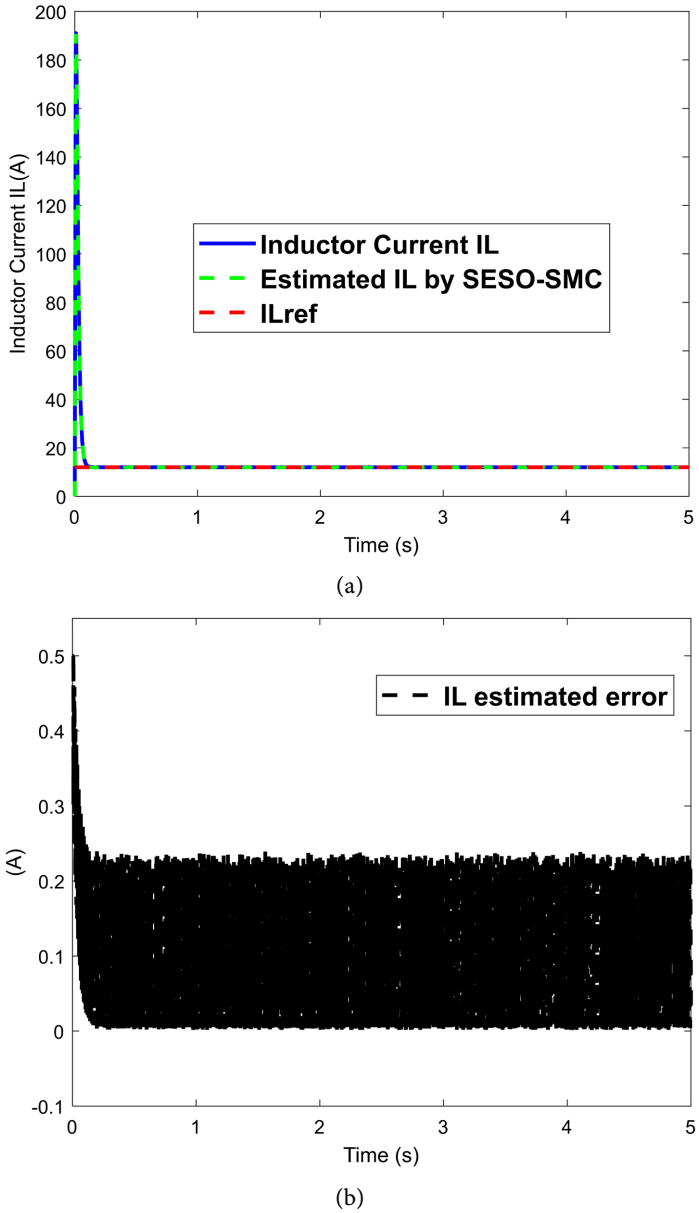


Figure 5. Response curves of the real and estimated boost converter inductor current (a) and estimation error (b) by the SESO and SMC combination methods.

Figure 6 displays the actual DC bus voltage estimated by combining SMC and SESO. From the estimated error curve, it tends to almost zero. This indicates that the estimated values are close to the actual values. The results demonstrate that the estimator accurately predicts the voltage of the DC bus.

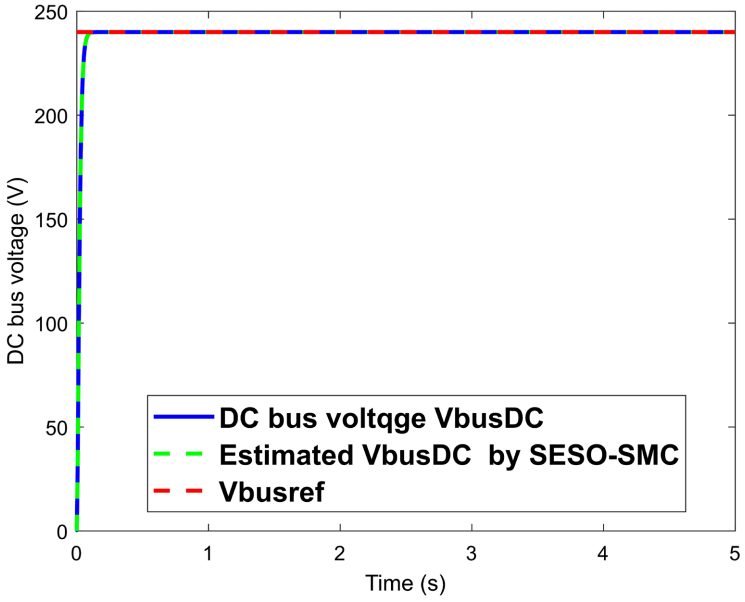


(a)

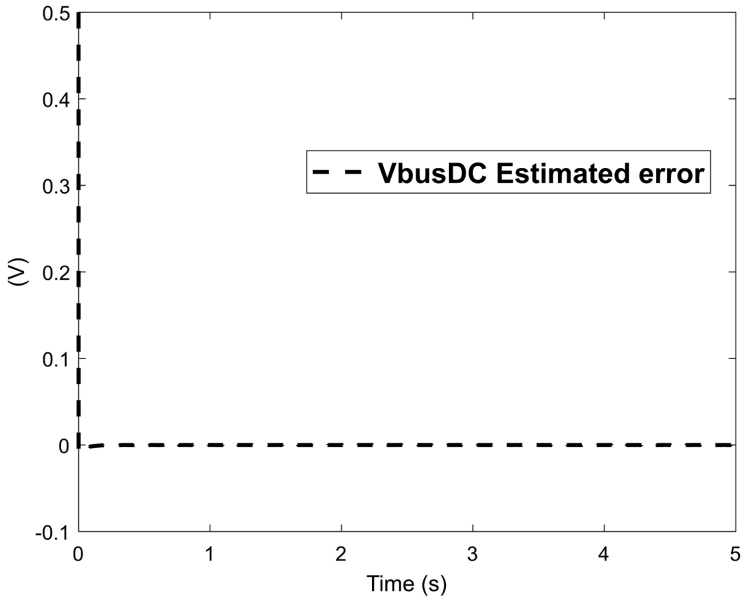


(b)

Figure 6. Response curves of the real and estimated DC bus voltage (a) and estimation error (b) by the SESO and SMC combination methods.

Figure 7 shows the real and estimated d1 disturbances of the system. The error curve tends to zero, with an order of $10^{-5}$. The estimated values obtained by the combination of SESO and SMC follow the real values of the disturbances d1.

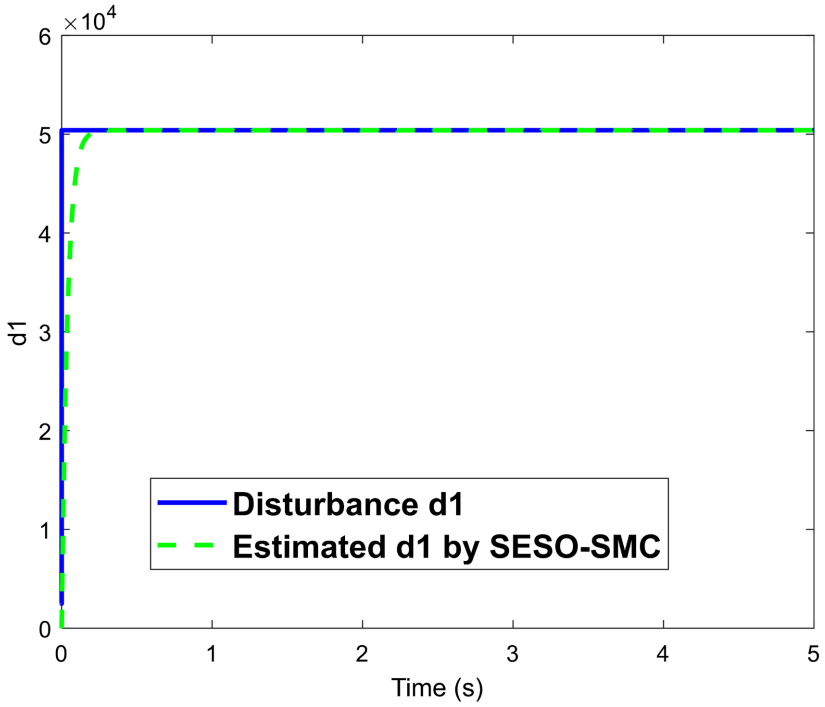


(a)

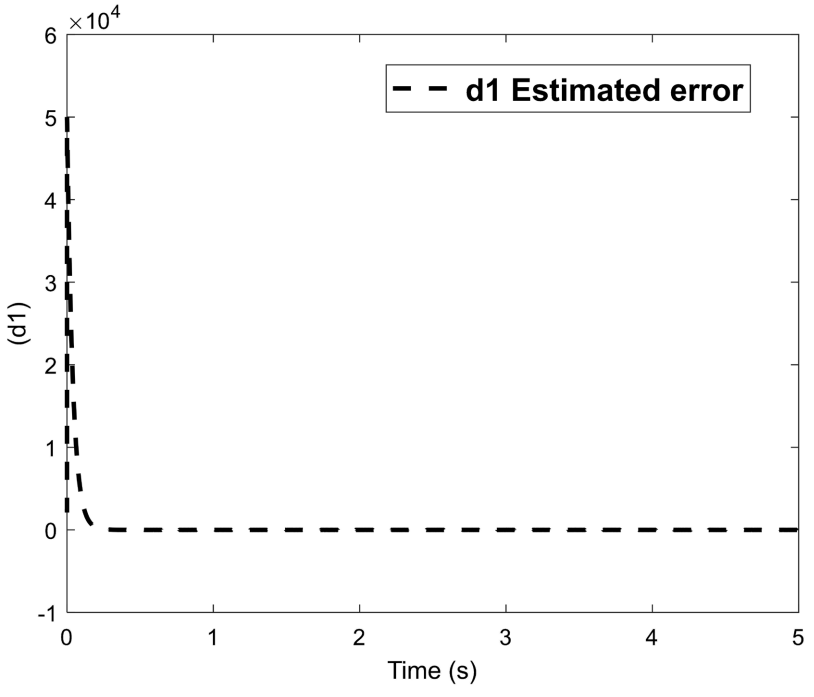


(b)

**Figure 7.** Real and estimated disturbance d1 and estimation error curves (a) and estimation error (b) by the SESO and SMC combination methods.

**Figure 8** shows the studied system's real and estimated d2 disturbances. The error curve tends to zero, with an order of $10^{-6}$. The values estimated by the combination of SESO and SMC align with the actual disturbances' values.

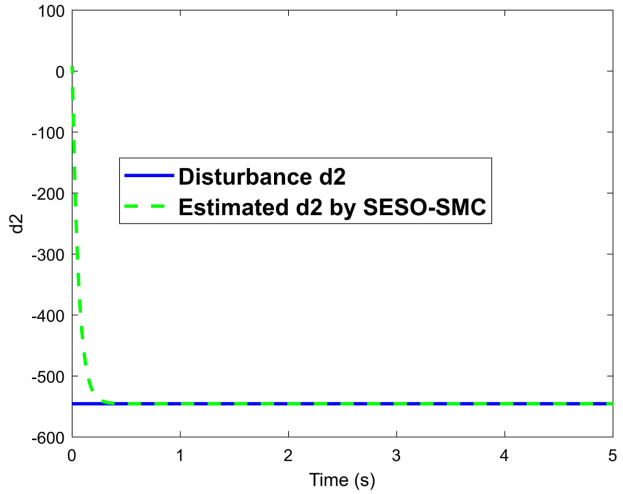


(a)

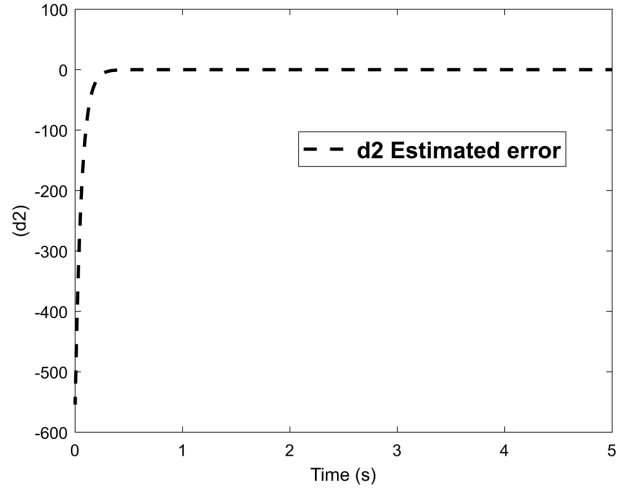


(b)

**Figure 8.** Real and estimated disturbance d2 and estimation error curves (a) and estimation error (b) by the SESO and SMC combination methods.

## 8.3. Robustness Test of the Combination Methods of SESO and SMC on the PV/Boost Converter/DC Load System

This section tests the robustness of the SESO and SMC combination methods against PV voltage and DC load disturbances.

### 8.3.1. Combination Methods of SESO and SMC Subjected to PV Voltage ($V_{pv}$) Perturbations

In this work, it is assumed that the voltage $V_{pv}$ is perturbed due to the clouds or for other mismatches and changes as follows:

$$V_{pv} = \begin{cases} 240 \text{ V, for } t \in [0;0.5[\text{ s} \\ 220 \text{ V, for } t \in [0.5;1[\text{ s} \\ 230 \text{ V, for } t \in [1;2[\text{ s} \\ 250 \text{ V, for } t \in [2;3[\text{ s} \\ 240 \text{ V, for } t \in [3;5]\text{ s} \end{cases} \quad (28)$$

Figure 9 illustrates the actual inductance current and estimated value generated by the combination of SMC and SESO, in the presence of external PV voltage perturbations. At the beginning of the variation time (0.5 s), the current is subject to oscillations (of small amplitude). The small oscillations of the estimated error range from 0.0 A to 0.5 A at all variation times (0.5 s, 1 s, 2 s, 3 s), resulting in a maximum relative error of 4%. This indicates that the estimated values are close to the actual values. The results demonstrate that the combined methods accurately predict the current, allowing effective tracking of the set reference, although PV voltage varies from the set reference (variation of maximum 20 V). So, the combined methods are robust to PV voltage variation while estimating inductance current.

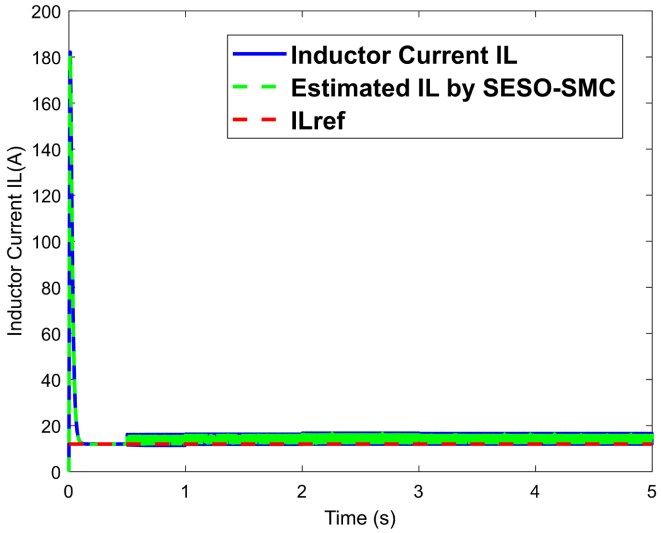


(a)

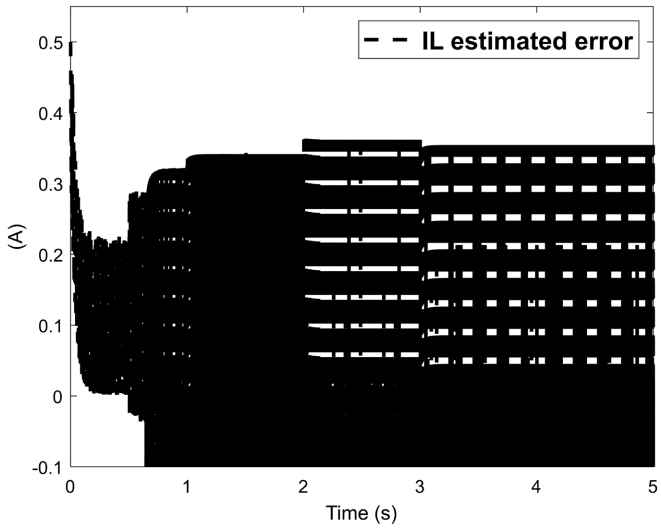


(b)

Figure 9. Response curves of the real and estimated boost converter inductance current (a) and estimation error (b) by the SESO and SMC combination methods, subjected to PV voltage variation.

Figure 10 displays the actual DC bus voltage estimated by combining SMC and SESO, in the presence of external PV voltage perturbations. From the estimated error curve, it tends to almost zero. The DC bus voltage is subject to oscillations (of tiny amplitude) while the PV voltage varies. The small oscillations of the estimated error are quietly zero, of the order of $10^{-4}$. This indicates that the estimated values are close to the actual values. The results demonstrate that combined methods accurately predict the current, allowing effective tracking of the set reference, although PV voltage varies from the set reference (variation of maximum 20 V). So, the combined methods are robust to PV voltage variation while estimating DC bus voltage.

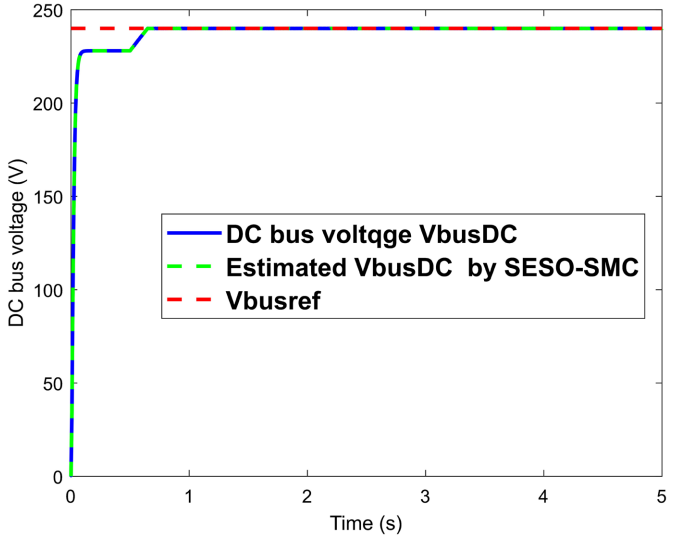


(a)

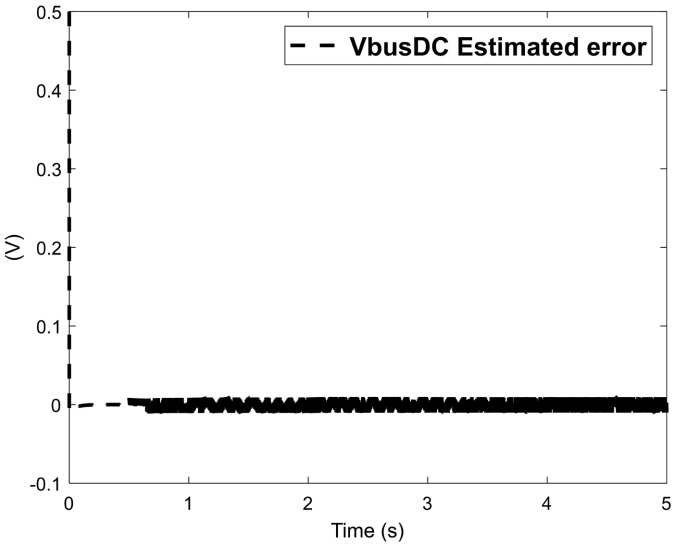


(b)

Figure 10. Response curves of the real and estimated DC bus voltage Vdc_bus (a) and estimation error (b) by the SESO and SMC combination methods subjected to PV voltage variation.

Figure 11 shows the system's real and estimated d1 disturbances in the presence of external PV voltage perturbations. The estimated d1 curve does not follow the real curve precisely. It takes the shape of the real curve but does not have closed values. The error curve reveals a gap between the real and estimated disturbances d1, with an order of $10^3$. When PV voltage varies, the estimated values obtained by combining SESO and SMC do not follow the real values of the disturbances d1, even though they take the form, resulting in a maximum relative error of 20%. So, the combined methods are not robust to PV voltage variation while estimating disturbances d1.

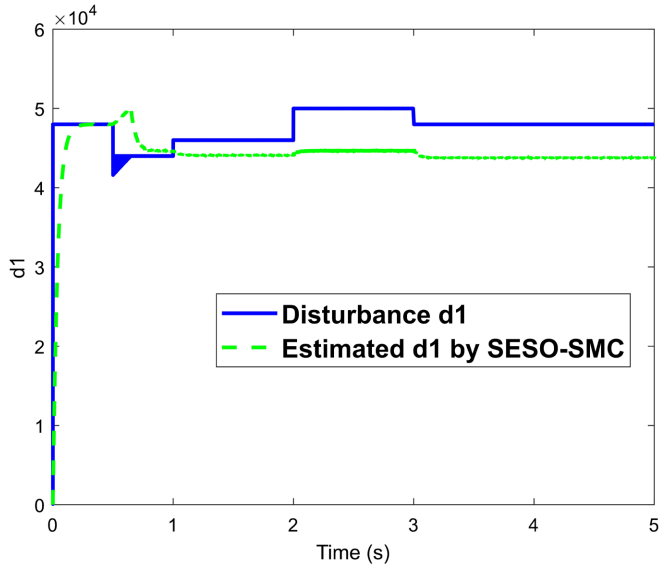


(a)

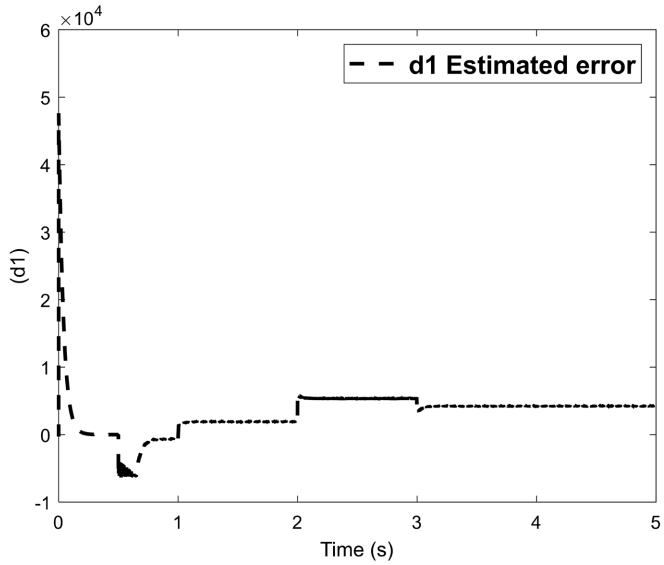


(b)

Figure 11. Real and estimated disturbance d1 and estimation error curves (a) and estimation error (b) by the SESO and SMC combination methods subjected to PV voltage variation.

Figure 12 shows the system's real and estimated d2 disturbances in the presence of external PV voltage perturbations. The estimated d2 curve follows the real curve. The disturbances d2 are subject to oscillations (of considerable amplitude) while the PV voltage varies. The error curve reveals a gap between the real and estimated disturbances d1, with an order of 100. When PV voltage varies, the estimated values obtained by combining SESO and SMC do not follow the real values of the disturbances d2, even though the real values oscillate with a considerable amplitude, resulting in a maximum relative error of 18%. So, the combined methods are not robust to PV voltage variation while estimating disturbances d2.

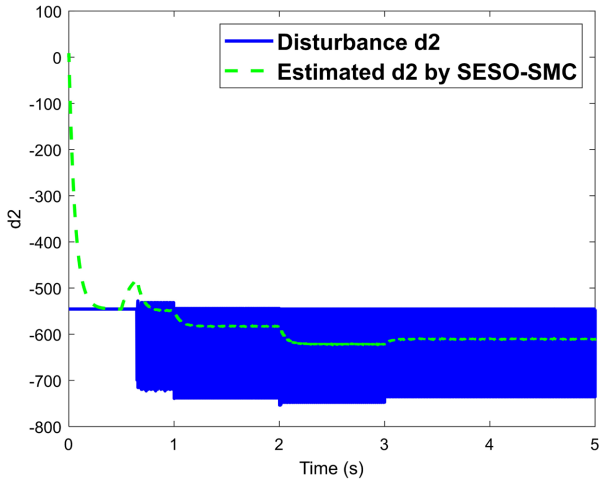


(a)

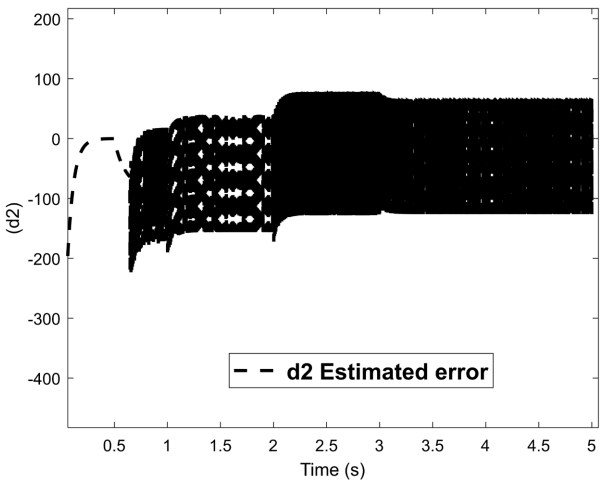


(b)

Figure 12. Real and estimated disturbance d2 and estimation error curves (a) and estimation error (b) by the SESO and SMC combination methods subjected to PV voltage variation.

### 8.3.2. Combination Methods of SESO and SMC Subjected to DC Load (Iload) Perturbations

In this work, it is assumed that the DC load current $I_{load}$ is perturbed, and changes as follows:

$$I_{load} = \begin{cases} 12 \text{ A, for } t \in [0;0.5[\text{ s} \\ 10 \text{ A, for } t \in [0.5;2[\text{ s} \\ 8 \text{ A, for } t \in [2;3]\text{s} \\ 12 \text{ A, for } t \in [3;5]\text{s} \end{cases} \quad (29)$$

Figure 13 illustrates the actual inductance current and estimated value generated by the combination of SMC and SESO, in the presence of external load current perturbations. At the beginning of the variation time (0.5 s), the current is subject to oscillations (of small amplitude). The small oscillations of the estimated error range from 0.0 A to 0.5 A at all variation times (0.5 s, 1 s, 2 s, 3 s), resulting in a maximum relative error of 4%. This indicates that the estimated values are close to the actual values. The results demonstrate that the combined methods accurately predict the current, allowing effective tracking of the set reference, although DC load current varies from the set reference (variation of maximum 4 A). So, the combined methods are robust to DC load current variation while estimating inductance current.

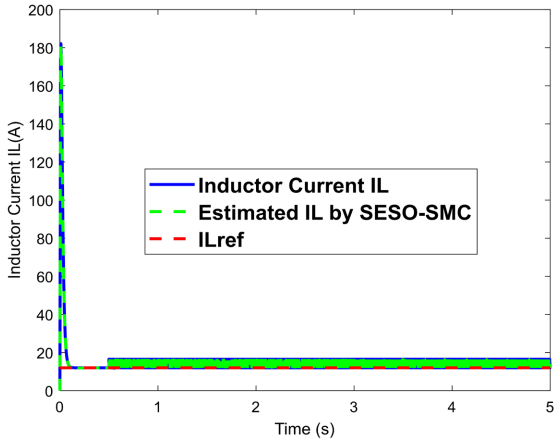


(a)

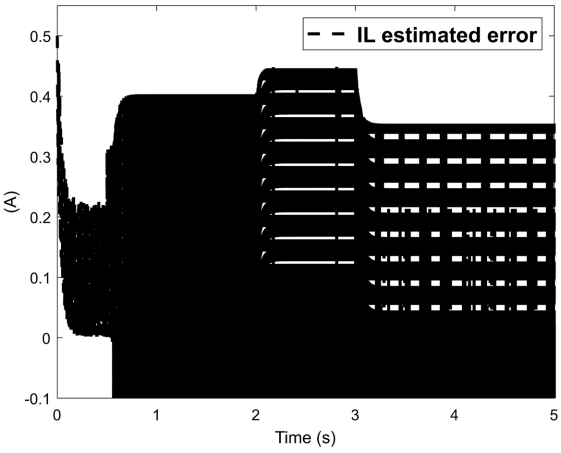


(b)

Figure 13. Response curves of the real and estimated boost converter inductance current (a) and estimation error (b) by the SESO and SMC combination methods subjected to DC load variation.

Figure 14 displays the actual DC bus voltage estimated by combining SMC and SESO, in the presence of external DC load current perturbations. From the estimated error curve, it tends to almost zero. The DC bus voltage is subject to oscillations (of tiny amplitude) while the DC load current varies. The small oscillations of the estimated error are quietly zero, of the order of $10^{-4}$. This indicates that the estimated values are close to the actual values. The results demonstrate that combined methods accurately predict the current, allowing effective tracking of the set reference, although DC load current varies from the set reference (variation of maximum 4 A). So, the combined methods are robust to DC load current variation while estimating DC bus voltage.

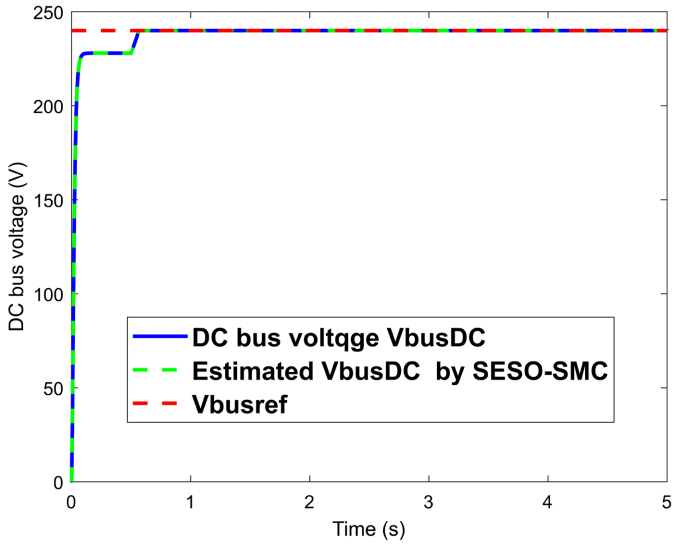


(a)

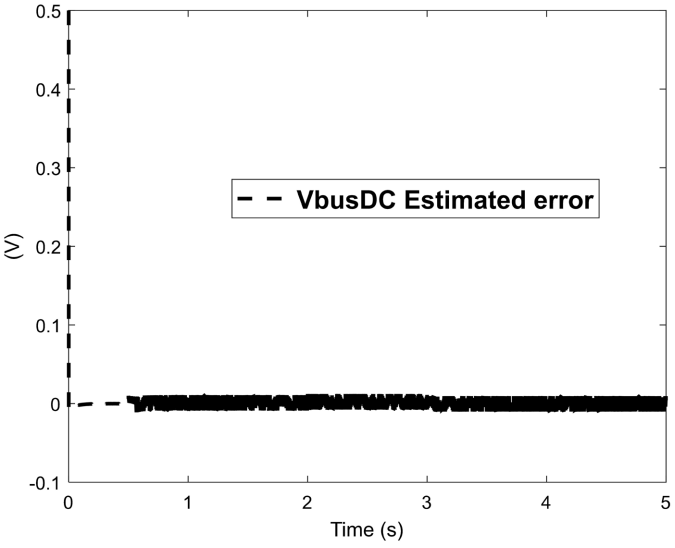


(b)

Figure 14. Response curves of the real and estimated DC bus voltage Vdc_bus (a) and estimation error (b) by the SESO and SMC combination methods subjected to DC load variation.

Figure 15 shows the system's real and estimated d1 disturbances in the presence of external DC load perturbations. The estimated d1 curve does not follow the real curve precisely. It does not take the form of the real curve. The error curve reveals a gap between the real and estimated disturbances d1, with an order of $2 \times 10^3$. When DC load current varies, the estimated values obtained by combining SESO and SMC do not follow the real values of the disturbances d1, resulting in a relative error of over 20%. So, the combined methods are not robust to DC load current variation while estimating disturbances d1.

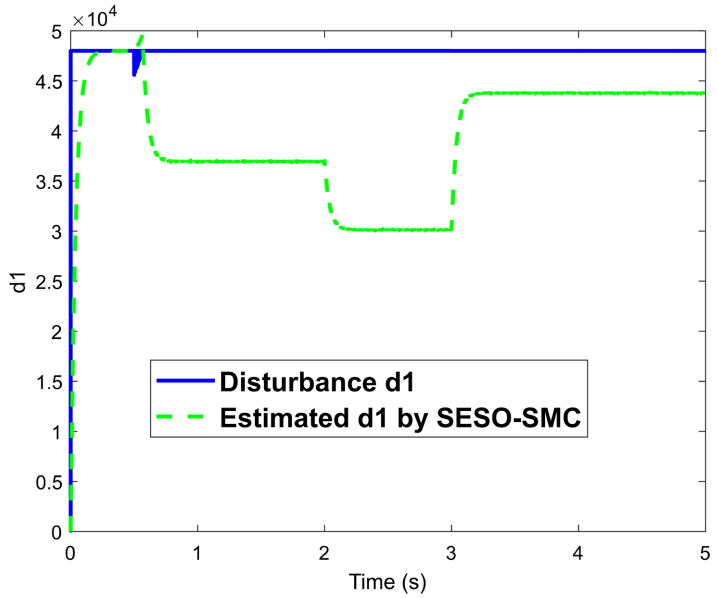


(a)

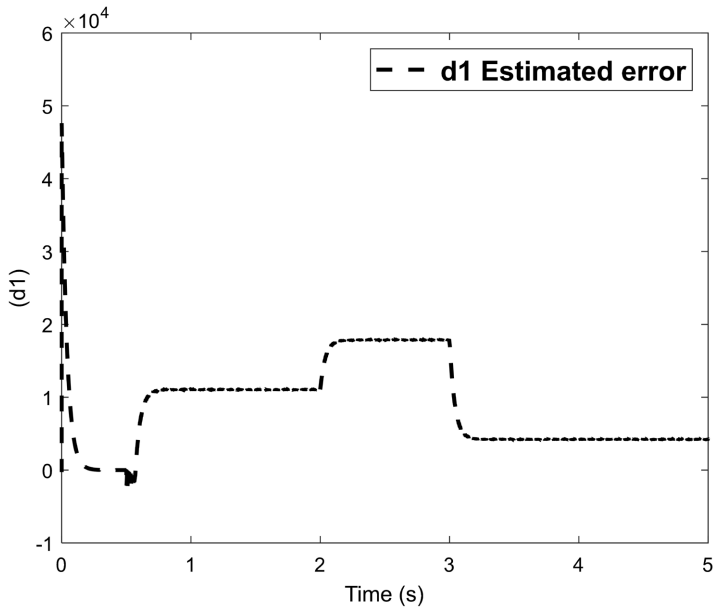


(b)

Figure 15. Real and estimated disturbance d1 and estimation error curves (a) and estimation error (b) by the SESO and SMC combination methods subjected to DC load variation.

Figure 16 shows the system's real and estimated d2 disturbances in the presence of external PV voltage perturbations. The estimated d2 curve follows the real curve. The disturbances d2 are subject to oscillations (of considerable amplitude) while the PV voltage varies. The error curve reveals a gap between the real and estimated disturbances d1, with an order of 200. When DC load current varies, the estimated values obtained by combining SESO and SMC follow the real values of the disturbances d2, even though the real values oscillate with a considerable amplitude, resulting in a relative error of over 30%. So, the combined methods are not robust to DC load current variation while estimating disturbances d2.

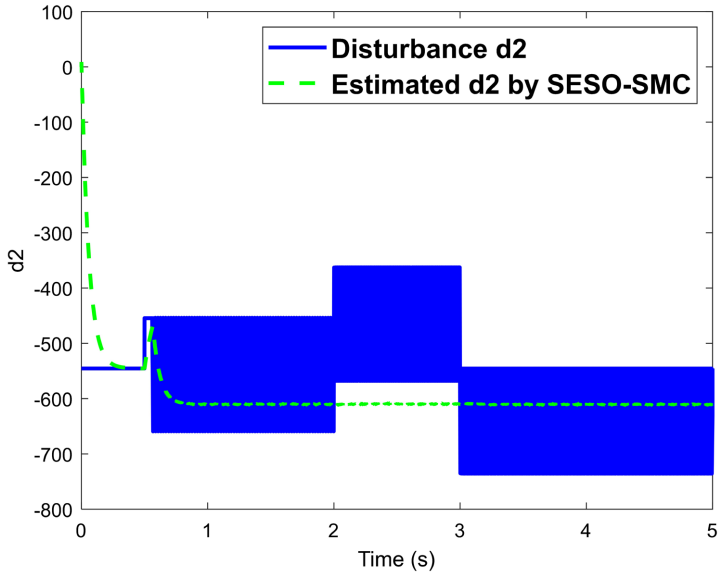


(a)

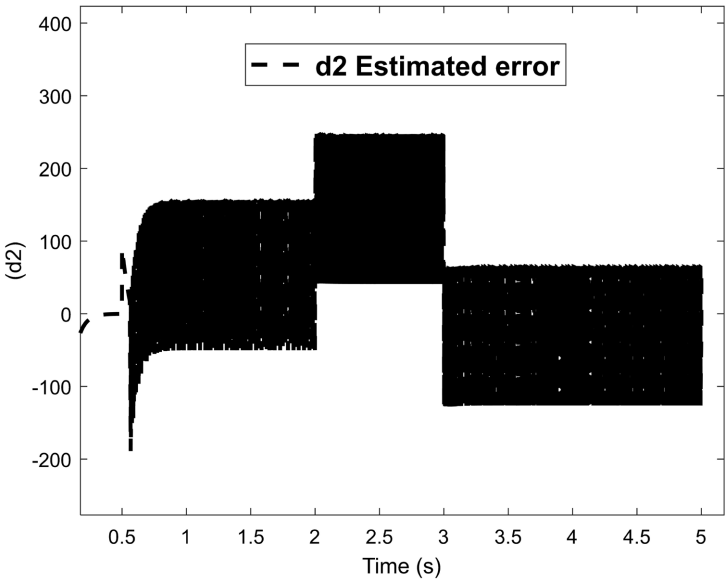


(b)

Figure 15. Real and estimated disturbance d1 and estimation error curves (a) and estimation error (b) by the SESO and SMC combination methods subjected to DC load variation.

The chattering phenomenon persists in the control law. This is due to the sign (.) function. To mitigate this high-frequency disturbance, several previous works were drawn upon [44]. This allowed us to replace the sign (.) function with the hyperbolic tangent tanh (.). It has also been observed that increasing the SMC parameter K reduces the chattering phenomenon in the control law.

### 8.4. Performance Indicators

Table 2 presents the quantitative performance indicators for the combination of the sliding mode control (SMC) and standard extended state observer (SESO) methods in estimating the states of a Photovoltaic system associated with a boost converter and DC load, subject to mismatched disturbances. This table explains and compares the performance indicators for each state in the absence and the presence of perturbations. Globally, these performance indicators show good robustness for the principal states (IL and Vbus_DC) and poor disturbance reconstruction for lumped state disturbances.

Table 2. Simulation performance indicators without/with perturbations.

| Performance indicators | | SMC with SESO | | | Comments |
|---|---|---|---|---|---|
| | | Without Perturbations | With voltage Perturbations | With Current Perturbations | |
| Settling time (s) 2% | Current IL (A) | 0.0774 s | 0.0714 s | 0.0586 s | The estimated values stabilise quickly, although perturbations |
| | voltage Vdc_bus (V) | 0.0671 s | 0.3172 s | 0.3173 s | The estimated values stabilise quickly, although perturbations |
| | disturbance d1 | 0.0934 s | 2.99 s | 3.0753 s | The estimated values stabilise after perturbation time |
| | disturbance d2 | 0.1375 s | 3.0128 s | 3.0242 s | The estimated values stabilise after perturbation time |
| Maximum overshoot | Current IL (A) | 178.89 A | 169.93 A | 169.93 A | The current peak exceeds the target (12 A) by 1416% to 1490.7% |
| | voltage Vdc_bus (V) | 0.0001 V | 0.0165 V | 0.0339 V | The voltage peak exceeds the target (240 V) by 0.00004% to 0.014% |
| | disturbance d1 | 8.1645e−04 | 2464 | 2459 | High peaks appear when perturbations occur |
| | disturbance d2 | 4.3996e−06 | 81.4184 | 2.7506 | Slightly peaks appear when perturbations occur |
| Mean Steady-state error | Current IL (A) | 0.07056 A | 0.01915 A | 0.014809 A | The control system tracks accurately the desired current IL |
| | voltage Vdc_bus (V) | 4.1617e−05 V | 5.1352e−05 V | 9.2216e−05 V | The control system tracks accurately the desired voltage Vdc_Bus |
| | disturbance d1 | 240.4364 | 3488.4949 | 9064.4041 | When perturbations occur, the control system fails to track the real values of disturbance d1 |

**Continued**

| | | | | | |
|---|---|---|---|---|---|
| | disturbance d2 | 3.9901 | 32.1266 | 95.0652 | When perturbations occur, the control system fails to track the real values of disturbance d2 |
| **RMSE of Disturbances estimates** | disturbance d1 | 2430.2912 | 4476.4741 | 10879.9526 | The performance of the model's predicted values degraded, highly, with perturbations. |
| | disturbance d2 | 33.6545 | 69.9825 | 136.5154 | The performance of the model's predicted values degraded, slowly, with perturbations. |

## 9. Conclusions

This paper explores the application of the combination of standard extended state observer (SESO) and the sliding mode control (SMC) approaches to the PV/controller/load system. The design and tuning of the gains for achieving good states stabilities are more structured. The global stability of the closed-loop system with the combined methods is guaranteed.

The results reveal that the combined methods are robust against perturbations from PV voltage variation and DC load current when estimating the principal states (inductance current IL and bus DC voltage). However, for the disturbance states (d1 and d2), the combined methods have difficulties accurately estimating the real values. The gaps observed are considerable, although the estimated values take the real form. Therefore, the mixed methods are robust for the principal states and not robust for the disturbances. Practically, the operators of the systems deal mainly with the principal states. These are worth putting into the health state evaluation of the whole system. The lumped states disturbances parts of the system can be estimated but are not indispensable for the operators. The operators must verify the stability of these parts of the systems.

To effectively track the disturbance parts, the Sliding Mode Control component will be enhanced with a fast estimator, such as a Generalised Extended State Observer (GESO) or Disturbance Observer-Based Control for nonlinear systems, which will be incorporated into future research work.

## Acknowledgements

The authors would like to acknowledge Department of Renewable Energy, National Advance School of Engineering of Maroua, University of Maroua.

## Author Contributions

Albert Ayang is the main author of this work. He wrote the first draft of the manuscript, the conception of the study and performed the results analysis. Etienne Tchoffo Houdji, Jean Benjamin Bidias, Yaouba, Fabrice Kwefeu Mbakop and Guy Bertrand Tchaya contributed to manuscript revision, read, and approved the submitted version.

## Conflicts of Interest

The authors declare that they have no known competing financial interests or personal relationships that could have appeared to influence the work reported in this paper.

## References


[1] Duman, T., Marti, S., Moonem, M., Abdul Kader, A. and Krishnaswami, H. (2017) A Modular Multilevel Converter with Power Mismatch Control for Grid-Connected Photovoltaic Systems. *Energies*, **10**, Article 698. https://doi.org/10.3390/en10050698

[2] Wang, J. and Sun, Y. (2024) Load Frequency Active Disturbance Rejection Control Based on Improved Particle Swarm Optimization. *Electronics*, **13**, Article 1268. https://doi.org/10.3390/electronics13071268

[3] Thakran, S., Singh, J., Garg, R. and Mahajan, P. (2018) Implementation of P&O Algorithm for MPPT in SPV System. 2018 *International Conference on Power Energy, Environment and Intelligent Control* (*PEEIC*), Greater Noida, 13-14 April 2018, 242-245. https://doi.org/10.1109/peeic.2018.8665588

[4] Halder, T. (2016) A Maximum Power Point Tracker (MPPT) Using the Incremental Conductance (INC) Technique. 2016 7*th India International Conference on Power Electronics* (*IICPE*), Patiala, 17-19 November 2016, 1-6. https://doi.org/10.1109/iicpe.2016.8079449

[5] Reddy, D. and Ramasamy, S. (2017) A Fuzzy Logic MPPT Controller Based Three Phase Grid-Tied Solar PV System with Improved CPI Voltage. 2017 *Innovations in Power and Advanced Computing Technologies* (*i-PACT*), Vellore, 21-22 April 2017, 1-6. https://doi.org/10.1109/ipact.2017.8244953

[6] Mohapatra, A., Nayak, B. and Saiprakash, C. (2019) Adaptive Perturb & Observe MPPT for PV System with Experimental Validation. 2019 *IEEE International Conference on Sustainable Energy Technologies* (*ICSET*), Bhubaneswar, 26 February-March 2019, 257-261. https://doi.org/10.1109/icsets.2019.8744819

[7] Yang, H.P., Jiang, Q.X. and Zhong, Y. (2010) Active-Disturbance Rejection Control and Its Application to Solar PV DC-DC Converter. 2010 3*rd International Conference on Advanced Computer Theory and Engineering* (*ICACTE*), Chengdu, 20-22 August 2010, V3-170-V3-173. https://doi.org/10.1109/icacte.2010.5579669

[8] Darbali-Zamora, R. and Ortiz-Rivera, E.I. (2019) An Overview into the Effects of Nonlinear Phenomena in Power Electronic Converters for Photovoltaic Applications. 2019 *IEEE* 46*th Photovoltaic Specialists Conference* (*PVSC*), Chicago, 16-21 June 2019, 2908-2915. https://doi.org/10.1109/pvsc40753.2019.8980933

[9] Prakash, S., Alkhatib, M. and Muduli, U.R. (2024) Active Disturbance Rejection Controller Approach for Boost Converter in PV Application. 2024 *IEEE International Conference on Power Electronics, Drives and Energy Systems* (*PEDES*), Mangalore, 18-21 December 2024, 1-6. https://doi.org/10.1109/pedes61459.2024.10961464

[10] Marhraoui, S., Abbou, A., Ziouh, A., hichami, N.E. and Rhaili, S.E. (2018) Robust Integral Backstepping Approach for MPPT in Different Models of Solar Panel. 2018 7*th International Conference on Renewable Energy Research and Applications* (*ICRERA*), Paris, 14-17 October 2018, 371-376. https://doi.org/10.1109/icrera.2018.8566783

[11] Fei, L. and Jiandi, Z. (2017) The MPPT Technology Based on Integral Sliding Mode Control. 2017 *IEEE International Conference on Information and Automation* (*ICIA*), Macao SAR, 18-20 July 2017, 288-292. https://doi.org/10.1109/icinfa.2017.8078921

[12] Hao, X., Yang, X., Liu, T., Huang, L. and Chen, W. (2013) A Sliding-Mode Controller with Multiresonant Sliding Surface for Single-Phase Grid-Connected VSI with an LCL Filter. *IEEE Transactions on Power Electronics*, **28**, 2259-2268. https://doi.org/10.1109/tpel.2012.2218133

[13] Vieira, R.P., Martins, L.T., Massing, J.R. and Stefanello, M. (2018) Sliding Mode Controller in a Multiloop Framework for a Grid-Connected VSI with LCL Filter. *IEEE Transactions on Industrial Electronics*, **65**, 4714-4723. https://doi.org/10.1109/tie.2017.2772143

[14] Komurcugil, H., Biricik, S., Bayhan, S. and Zhang, Z. (2021) Sliding Mode Control: Overview of Its Applications in Power Converters. *IEEE Industrial Electronics Magazine*, **15**, 40-49. https://doi.org/10.1109/mie.2020.2986165

[15] Naddami, S. and Ababssi, N. (2024) Robust Control and Energy Management in Grid-connected Photovoltaic-Battery Energy Storage Systems. *International Journal of Intelligent Engineering & Systems*, **17**, 368-379.

[16] Kim, K., Park, J. and Choi, Y. (2006) Chattering Free Sliding Mode Control. 2006 *SICE-ICASE International Joint Conference*, Busan, 18-21 October 2006, 732-735. https://doi.org/10.1109/sice.2006.315237

[17] Han, J.Q. (1998) Auto Disturbance Rejection Controller and It's Applications. *Control and Decision*, **13**, 19-23.

[18] Han, J. (2009) From PID to Active Disturbance Rejection Control. *IEEE Transactions on Industrial Electronics*, **56**, 900-906. https://doi.org/10.1109/tie.2008.2011621

[19] Aboudrar, I., El Hani, S., Heyine, M.S. and Naseri, N. (2019) Dynamic Modeling and Robust Control by ADRC of Grid-connected Hybrid PV-Wind Energy Conversion System. *Mathematical Problems in Engineering*, **2019**, Article ID: 8362921. https://doi.org/10.1155/2019/8362921

[20] Singh, J.K., Prakash, S., Al Jaafari, K., Al Zaabi, O., Al Hosani, K., Behera, R.K., *et al.* (2023) Active Disturbance Rejection Control of Photovoltaic Three-Phase Grid Following Inverters under Uncertainty and Grid Voltage Variations. *IEEE Transactions on Power Delivery*, **38**, 3155-3168. https://doi.org/10.1109/tpwrd.2023.3266898

[21] Eker, D. and Özbek, N.S. (2021) An Assessment of Active Disturbance Rejection Technique from a Theoretical Perspective. *European Journal of Science and Technology*, No. 29, 284-291. https://doi.org/10.31590/ejosat.1024241

[22] Gao, Z. (2003) Scaling and Bandwidth-Parameterization Based Controller Tuning. *Proceedings of the* 2003 *American Control Conference*, 2003, Denver,4-6 June 2003, 4989-4996.

[23] Gao, Z.Q. (2006) Active Disturbance Rejection Control: A Paradigm Shift in Feedback Control System Design. 2006 *American Control Conference*, Minneapolis, 14-16 June 2006, 7. https://doi.org/10.1109/acc.2006.1656579

[24] Kharrat, D., Gassara, H., El Hajjaji, A. and Chaabane, M. (2018) Adaptive Observer and Fault Tolerant Control for Takagi-Sugeno Descriptor Nonlinear Systems with Sensor and Actuator Faults. *International Journal of Control, Automation and Systems*, **16**, 972-982. https://doi.org/10.1007/s12555-017-0546-8

[25] Zhang, H., Han, J., Wang, Y. and Liu, X. (2017) Sensor Fault Estimation of Switched Fuzzy Systems with Unknown Input. *IEEE Transactions on Fuzzy Systems*, **26**, 1114-1124. https://doi.org/10.1109/tfuzz.2017.2704543

[26] Li, M., Liu, M., Zhang, Y. and Geng, Y. (2018) Fault Tolerant Sliding Mode Control for T-S Fuzzy Stochastic Time-Delay System via a Novel Sliding Mode Observer Approach. *International Journal of Systems Science*, **49**, 1353-1367.

https://doi.org/10.1080/00207721.2018.1447168

[27] Benyamina, F., Benrabah, A., Khoucha, F., Zia, M.F., Achour, Y. and Benbouzid, M. (2021) An Augmented State Observer-Based Sensorless Control of Grid-Connected Inverters under Grid Faults. *International Journal of Electrical Power & Energy Systems*, **133**, Article ID: 107222. https://doi.org/10.1016/j.ijepes.2021.107222

[28] Li, X., Yan, J. and Yang, G. (2019) Adaptive Fault Estimation for T-S Fuzzy Interconnected Systems Based on Persistent Excitation Condition via Reference Signals. *IEEE Transactions on Cybernetics*, **49**, 2822-2834. https://doi.org/10.1109/tcyb.2018.2820001

[29] Mokhlis, M., Ferfra, M. and Idrissi, R. (2020) High Gain Observer-Based Control for Grid-Connected PV System under Partial Shading Effect. *International Journal of Intelligent Engineering and Systems*, **13**, 161-172. https://doi.org/10.22266/ijies2020.0430.16

[30] idrissi, R., Abbou, A. and Mokhlis, M. (2020) Backstepping Integral Sliding Mode Control Method for Maximum Power Point Tracking for Optimization of PV System Operation Based on High-Gain Observer. *International Journal of Intelligent Engineering and Systems*, **13**, 133-144. https://doi.org/10.22266/ijies2020.1031.13

[31] Stitou, M., Fadili, A.E., Chaoui, F.Z. and Giri, F. (2019) Adaptive High Gain Observer for Photovoltaic Systems. 2019 4*th World Conference on Complex Systems* (*WCCS*), Ouarzazate, 22-25 April 2019, 1-6. https://doi.org/10.1109/icocs.2019.8930772

[32] Adil, A., Hamaz, A., N'Doye, I., Zemouche, A., Laleg-Kirati, T. and Bedouhene, F. (2022) On High-Gain Observer Design for Nonlinear Systems with Delayed Output Measurements. *Automatica*, **141**, Article ID: 110281. https://doi.org/10.1016/j.automatica.2022.110281

[33] Adil, A., N'Doye, I. and Laleg-Kirati, T. (2022) High-Gain Observer Design for Nonlinear Systems with Delayed Output Measurements Using Time-Varying Gains. 2022 *IEEE* 61*st Conference on Decision and Control* (*CDC*), Cancun, 6-9 December 2022, 235-240. https://doi.org/10.1109/cdc51059.2022.9992555

[34] Barzegar-Kalashani, M. and Mahmud, M.A. (2022) A Linear Hybrid Active Disturbance Rejection Controller Design to Extenuate Powerline Bushfires in Resonant Grounded Distribution Power Systems. *International Journal of Electrical Power & Energy Systems*, **142**, Article ID: 108192. https://doi.org/10.1016/j.ijepes.2022.108192

[35] Zhang, X., Chen, Y. and Sun, X. (2023) Overview of Active Disturbance Rejection Control for Permanent Magnet Synchronous Motors. *Journal of Electrical Engineering & Technology*, **19**, 1237-1255. https://doi.org/10.1007/s42835-023-01710-w

[36] Ayang, A. (2020) Diagnostic d'un système photovoltaïque à stockage par estimation paramétrique et commandes ADRC, intégré à une centrale autonome de cogénération d'énergie. Master's Thesis, Université du Québec à Chicoutimi.

[37] Ayang, A., Saad, M., Ouhrouche, M. and Wamkeue, R. (2018) Modeling, P&O MPPT and PI Controls and Performance Analysis of PV/Energy Storage Hybrid Power System. 2018 4*th International Conference on Renewable Energies for Developing Countries* (*REDEC*), Beirut, 1-2 November 2018, 1-6. https://doi.org/10.1109/redec.2018.8597744

[38] Kassakian, J.G., Schlecht, M.F. and Verghese, G.C. (200) Principles of Power Electronics. Cambridge University Press.

[39] Boldea, I. and Tutelea, L.N. (2009) Electric Machines: Steady State, Transients, and Design with MATLAB. CRC Press.

[40] Guo, B. and Zhao, Z. (2016) Active Disturbance Rejection Control for Nonlinear Systems. Wiley. https://doi.org/10.1002/9781119239932

[41] Chen, Z., Sun, M. and Yang, R. (2014) On the Stability of Linear Active Disturbance Rejection Control. *Acta Automatica Sinica*, **39**, 574-580. https://doi.org/10.3724/sp.j.1004.2013.00574

[42] Slotine, J.J.E. and Li, W. (1991) Applied Nonlinear Control. Prentice Hall.

[43] Jain, P., Jian, L., Poon, J., Spanos, C., Sanders, S.R., Xu, J., *et al.* (2017) A Luenberger Observer-Based Fault Detection and Identification Scheme for Photovoltaic DC-DC Converters. *IECON* 2017—43*rd Annual Conference of the IEEE Industrial Electronics Society*, Beijing, 29 October-1 November 2017, 5015-5020. https://doi.org/10.1109/iecon.2017.8216866

[44] Belobo Mevo, B. (2019) Contribution à la commande adaptive et robuste d'un robot mobile de type unicycle avec modèle non-linéaire. Ph.D. Thesis, Université du Québec en Abitibi-Témiscamingue.